Hindawi
Advances in Civil Engineering
Volume 2019, Article ID 8106041, 19 pages
https://doi.org/10.1155/2019/8106041

Research Article

Experimental and Numerical Study on the Capability Behavior of a Thick-Walled Spatial Cast-Steel Joint under Complex Load Conditions

Binghan Zhang,[1] **Bin Yang**,[1] **Tiankai Wu**,[2] **Dayu Zhu**,[1] **and Ke Lei**[2]

[1]*Department of Structural Engineering, Tongji University, Shanghai 200092, China*
[2]*China Construction Eighth Engineering Division Corp. Ltd., Shanghai, China*

Correspondence should be addressed to Bin Yang; yangbin@tongji.edu.cn

Received 8 May 2019; Revised 8 July 2019; Accepted 29 July 2019; Published 28 August 2019

Academic Editor: Pier Paolo Rossi

A cast-steel joint is always used as an important component for the safety of the whole structure at key points, and the capability of the joint is important for the cast-steel joint. This paper conducts an experimental and numerical study on a 1/2 scale model of a joint in a real project. The experiment is used to validate the numerical model and then make further studies on the behavior of the joint by using a numerical method. Combining the result of the scale model test and numerical analysis shows that the joint can bear the prescribed load and it is still in the elastic stage. This paper also discusses the influence of the absence of the secondary moment, torque, and shear force. For the core area of the joint, the secondary moment and torque have little effect on the stress distribution, and the axial force of the secondary branches can increase the capability of the joint. But the secondary shear forces do have some effect on the stress of core area, and an enhancement coefficient is used to enlarge the axial force and moment to cover the absence of shear in the test.

1. Introduction

Cast-steel members are widely used in many major projects. It can be used as stiffeners, connectors, or joints in the steel structure. Cast-steel members have obvious advantages. They are more flexible, cheap, and more convenient for connection purposes. At the same time, cast-steel members can also be used to produce items with a more compact size [1]. Cast-steel members have a better seismic behavior [2–4]. Cast-steel joint is one of the most useful forms of the cast-steel members. It is often used in the key areas of structure for the following reasons: first, using cast-steel joints can avoid welding at the intersection of the members or move the welding area away from the joint area to prevent welding defects, residual stresses, and thermal deformation caused by welding [5]. Second, cast-steel joint can also reduce the difficulty in construction and improve safety [6]. Third, cast-steel nodes exhibit better fatigue performance than other alternatives [7]. Under cycle loads, some cast-steel members have properties of stress strengthening [8]. Cast-steel also has a better fire resistance, and its mechanical properties obviously changes when exposed to temperature exceeding 700°C [9]. Although the cast-steel has excellent mechanical performance, the ductility of the cast-steel is less than that of the normal steel [10].

Cast-steel joints are widely used, and the researches on cast-steel joints have made a lot of progress. Du et al. [6] performed research on tree-like column cast-steel joints and summed up a formula for predicting the capacity of cast-steel joints with branches under eccentric forces through an experiment and numerical analysis. Similarly, Du et al. [11] also carried out a numerical study on a tree-like cast-steel joint with three branches about the failure mode of the joint. Song et al. [12] presented an experiment on a huge cast-steel joint and verified the capability of the joint.

This paper conducts an experimental and numerical study on a 1/2 scale model based on a joint in a real project. The project is performed at a culture center, and it has a large-span floor system. The floor structure is supported by four concrete core tubes with concealed steel trusses. The span of the floor and trusses is up to 101.3 m, the height is only 6.3 m, and the height-span ratio is about 1/16. In this

project, the cast-steel joints are used to connect the main truss and the core tube as shown in Figure 1. This study takes one of the cast-steel joints as the prototype. The joint connects multiple members, under a complex load condition, and the force transferring path is not clear. It is a key component of the structure, directly related to the safety of the building.

Figures 2 and 3 show the details of the joint. Figures 2(a) and 3 are in the same direction. N8 and N7 are embedded in the core tube, so they can be regarded as fixed. N1–N4 are the main members, and N5 and N6 are considered as the secondary members. To ensure that the joint can satisfy the requirement of the construction project, an experiment based on a 1/2 scale model of the cast-steel joint was carried out according to *Technical Specification for Application of Connections of Structural Steel Casting* [13]. The specification demands that for the important joint which influences the safety of the entire structure or for complex connection, a test must be carried out to validate the capability and safety of the joint. And a finite element simulation must be used for assisting the real test as a contrast.

Although it is a 1/2 scale model test, the thickness of the test specimen in this experiment is still up to 150 mm. It is rare in cast-steel joints. In existing researches, most of the cast-steel joints do not have a thick cross section. Only few researches are about the thick cast-steel joints, and the thickness is no more than 80 mm. Existing research also advises that the thickness of the joint should be less than 150 mm [4]. This research can show the behavior of the thick-walled cast-steel joint.

Scale model experiment is a common method for huge joints. To make it possible for the loading equipment to exert the load, the joint can be scaled and the minimum scale of the prototype is 1/2 based on the request of the code [13]. It is obvious that the employment of similitude theory can save considerable expense and time. Ramu et al. [14] carried out an analytical investigation for the scale model test and provided a useful tool for solving the relevant problems. Chang et al. [15] conducted a study on piers failing in shear by using the reduced scale specimens. However, the scale model of the huge joint can still be very huge for the experiment, and it will be difficult to load until failure.

The combination of the real test and the finite element (FE) model is a good method to understand the behavior of complex joints. This method can also help carry out further study on the elastic stage of the joint and the distribution of the stress when it is difficult to measure the stress. Wang et al. [16] presented a method to compare the calculated surface stresses with those obtained from the experiment, to validate the FE model, and then to judge the stress distribution inside the joint by using the FE model at the same time. In this method, the experiment is mainly used for the verification of the FE model, and we can use the verified model to solve the problem that is difficult in the real experiment. Similarly, Su et al. [17] presented a method combining nondestructive field tests and the FE simulation to judge the capability of the joint through the stress increments in large-span spatial structures. Liu et al. [18] carried out numerical simulations for the scaled test on a T-joint and received a good agreement between the tests and simulation. Jahangiri et al. [19] used a numerical simulation method to study the cyclic responses of an innovative connection for beam and column.

In this paper, we conduct an experiment to validate the numerical model, and then make further studies on the behavior of the joint by using a numerical method. The influence of the secondary load to the capability of the joint is also discussed by using the numerical method. This part mainly discusses how the secondary moment, torque, shear, and axial force from the secondary branches of the joint influence the stress distribution of the core area of the joint.

2. Test Program

2.1. Test Specimen and Reaction Frame. The test specimen is 1/2 scale model of the real joint in the construction project. Only one specimen is tested in the experiment. The material of the test specimens is G20Mn5QT cast-steel. The material properties are obtained from a tensile experiment listed in Table 1.

The sizes and details of the prototype can be seen in Figure 4. To suit the need of the stress equivalence principle, the load applied to the specimen should be 1/4 of the designed value. The value of the load combinations can be seen in Table 2. It is the most unfavorable load combination provided by the designer of the structure, including the dead load, live load, and seismic load. Considering it is very difficult to apply all the loads, some of the design loads are considered as the secondary load. A preliminary FE analysis is also used to distinguish the secondary load. A reaction frame is designed for the test based on the geometric characteristics and load of the joint. It is a spatial self-balance reaction frame. Figure 5(c) shows the model of the reaction frame. Figures 5(a) and 5(b) are the real pictures of the reaction frame and cast-steel joint.

2.2. Loading Procedure. N7 and N8 are embedded in the core tube. In the experiment, they can be regarded as fixed boundary and do not need to be loaded. To reduce the difficulty of the test, the load should be simplified. First, N5 is a secondary member of the joint and its load is much smaller than the main members. So it can be ignored, and only N1–N4 are needed to be loaded.

Compared with the moment and axial force, the torque and the shear are secondary loads too. They can also be ignored in the test, and in Section 4, we will make further discussion about the absence of the secondary loads. The moment can be replaced by an eccentricity in the test.

The loading procedure is a monotonic loading. Before the formal loading, a preloading was conducted to make sure the test specimen can have a good contact and work normally. During the preloading, the equipment and instruments can also be tested. The load value of preloading is only 50% of the designed value, and the loading procedure is divided into 5 levels; for each time, 10% of the designed value, is loaded. Each level of the loading continues for 5 minutes. The unloading of the preloading is divided into 2

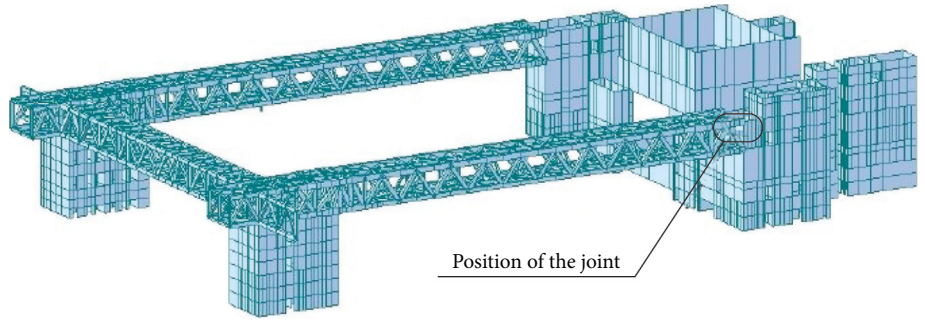

Figure 1: The position of the joint.

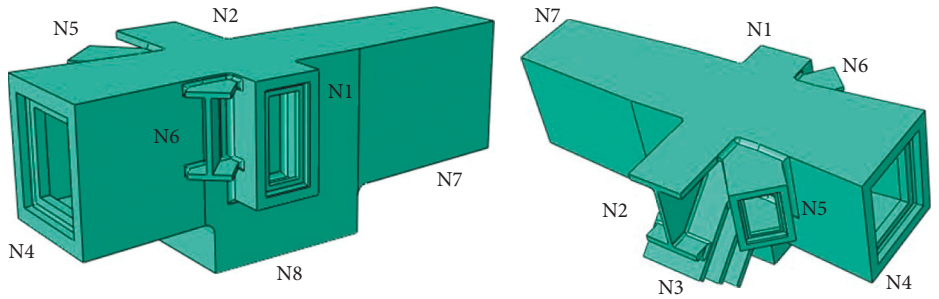

Figure 2: The cast-steel joint.

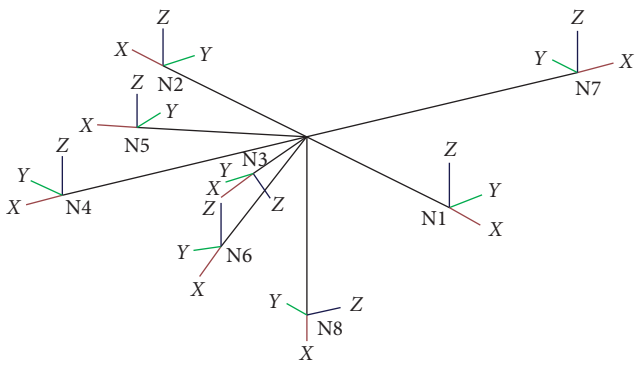

Figure 3: The number and local coordinate of the members.

Table 1: The material properties.

	G20Mn5QT
Yield strength (MPa)	385
Tensile strength (MPa)	555
Elongation (%)	26
Elastic modulus (MPa)	206000

steps, and fir each time, 25% is unloaded. The formal loading is controlled by 0.1 times of the designed value. And when the loading of all N1–N4 is 1.3 times of the designed value, continue loading N4 until it is 1.5 times of the designed value. Increasing the load on N4 can ensure the safety of the joint. The determination of this coefficient will be further discussed in Section 4.4 later. The load level is listed in Table 3, and the axial load of N4 is loading eccentricity to replace the moment load.

During the loading procedure, the data of the strain gauge and displacement meter will be collected by the computer constantly. The failure refers to the following criteria: (1) the specimen has obvious cracking; (2) the axial forces stop increasing when the loading procedure continues. If there is local buckling, the joint will also be regarded as damaged and the loading process will be stopped, but because of the thickness of the joint, it is almost impossible for the joint to buckle. The loading and unloading levels are listed in Table 3.

2.3. Measurement of Strain and Displacement. Strain gauge and displacement meter are used to measure the strain and displacement. There are totally 41 three-direction rosette strain gauges for the measurement of the von Mises stress in the test. And 22 single-direction strain gauges are also used to obtain stress. 3 displacement meters are set to measure the displacement of the main branch of the joint. The location of the strain gauges is shown in Figure 6.

3. Analysis and Discussion of the Results

During the loading procedure, the measured axial forces of N1–N4 are shown in Table 4, and the value of the load is listed in Table 4 (1.3 times of the designed value).

It can be seen in Figure 7 that, for most of the time, the measured value and the designed value of the load match well, but at level 1.0, the loading is not stable for N1 and N2. From load level 1.3 to 1.5, the load of N4 increases and the loads of N1–N3 are also influenced by N4. But it does not influence the result much because N4 is always stable and N4

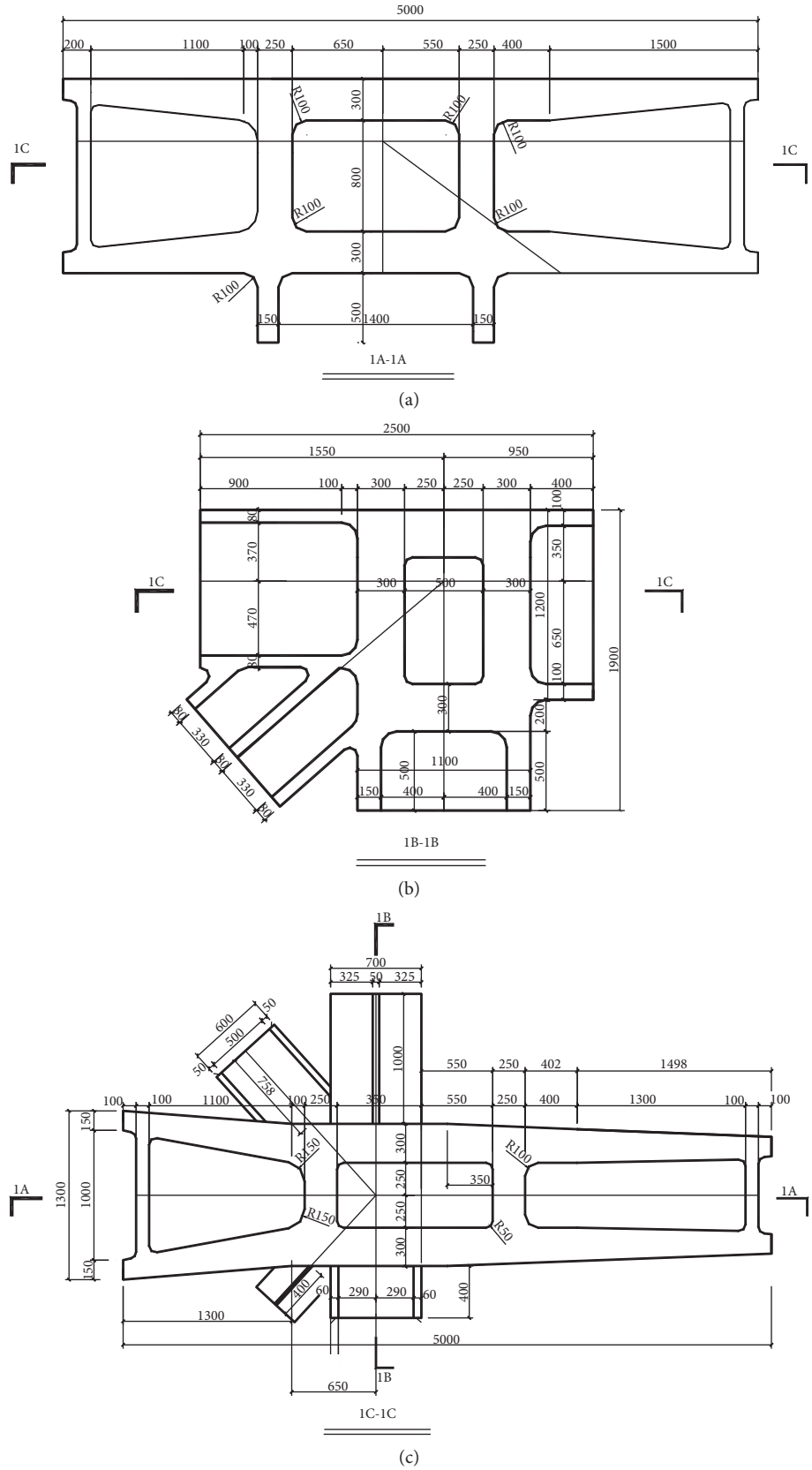

Figure 4: Detailed measurement of the test specimen.

Table 2: The designed value of the load (1/2 scale).

Unit number	Axial force (kN)	Shear-y (kN)	Shear-z (kN)	Torque (kN·m)	Moment-y (kN·m)	Moment-z (kN·m)
N1	3899.0	239.0	−333.0	−44.0	−256.0	−48.0
N2	2334.0	17.0	16.0	0.0	−136.0	25.0
N3	1492.0	26.0	37.0	0.0	38.0	−25.0
N4	17158.0	−642.0	1930.0	−242.0	−1930.0	−298.0
N5	1010.0	26.0	36.0	−7.0	−17.0	18.0
N7	12008.0	226.0	−752.0	−77.0	−1511.0	162.0
N8	−5565.0	204.0	305.0	1.0	−507.0	−114.0

(a) (b)

(c)

Figure 5: The reaction frame.

Table 3: The load procedure.

	Number	N1 (kN)	N2 (kN)	N3 (kN)	N4 (kN)
Loading	1	389.9	233.4	149.2	1715.8
	2	779.8	466.8	298.5	3431.6
	3	1169.8	700.2	447.7	5147.4
	4	1559.7	933.5	596.9	6863.2
	5	1949.6	1166.9	746.2	8579
	6	2339.5	1400.3	895.4	10294.8
	7	2729.5	1633.7	1044.6	12010.6
	8	3119.4	1867.1	1193.8	13726.4
	9	3509.3	2100.5	1343.1	15442.2
	10	3899.2	2333.8	1492.3	17158
	11	4289.2	2567.2	1641.5	18873.8
	12	4679.1	2800.6	1790.8	20589.6
	13	5069.0	3034.0	1940.0	22305.4
	14	5069.0	3034.0	1940.0	24021.2
	15	5069.0	3034.0	1940.0	25737
Unloading	1	4055.2	2427.2	1552	20589.6
	2	3041.4	1820.4	1164	15442.2
	3	2027.6	1213.6	776	10294.8
	4	1013.8	606.8	388	5147.4
	5	0.0	0.0	0.0	0.0

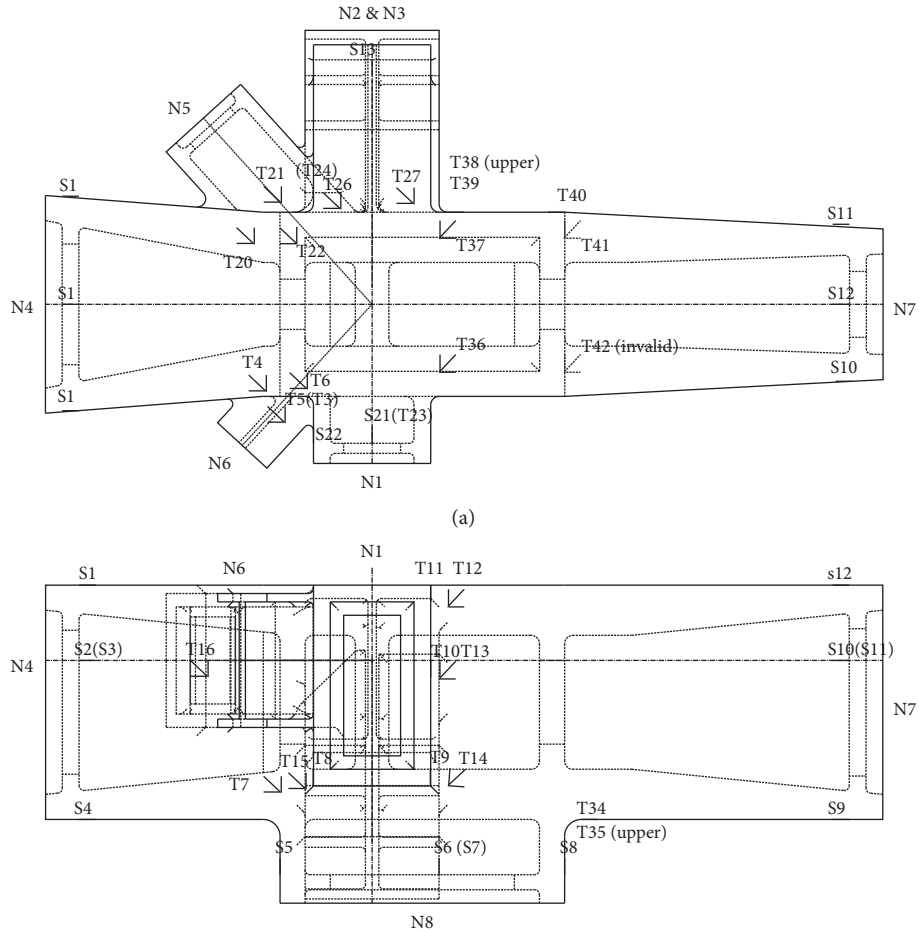

Figure 6: Continued.

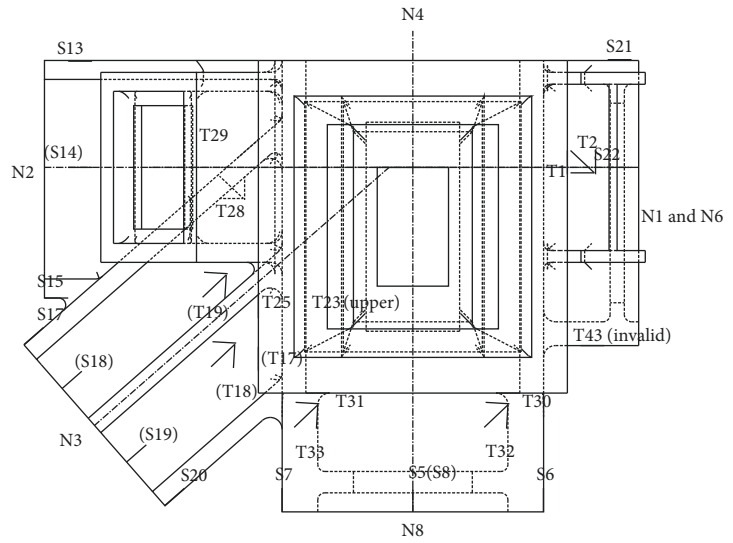

(c)

Figure 6: Arrangement of the strain gauge.

Table 4: The theoretical and measured forces of loading.

Number	Axial forces (kN)	Scale model axial forces (kN)	Measured axial forces (kN)	Deviation (%)
N1	15597	5068.7	4902.1	3.2
N2	9334	3034.2	3240.8	6.8
N3	5969	1939.6	1699.3	12.4
N4	68633	22305.4	22313.8	0.04
N4 (1.5 times)	79192	25737	25946.8	0.8

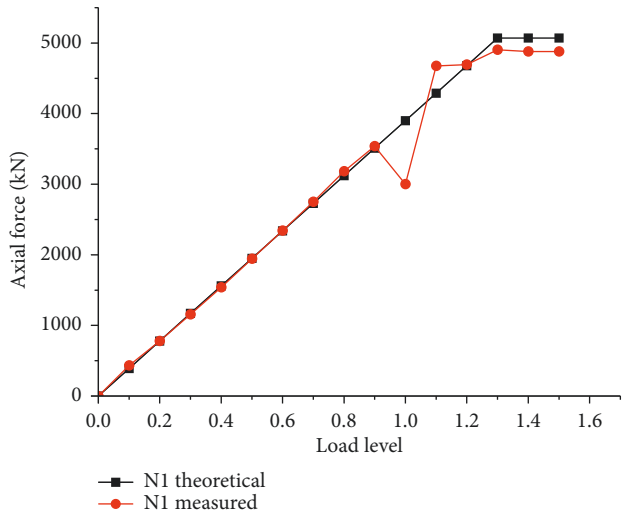

(a)

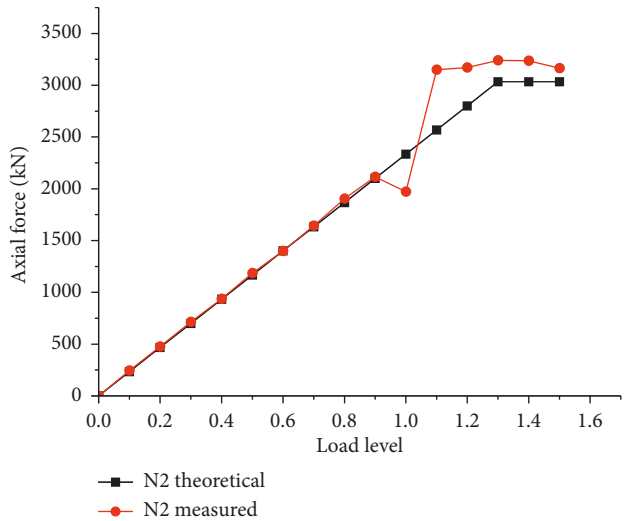

(b)

Figure 7: Continued.

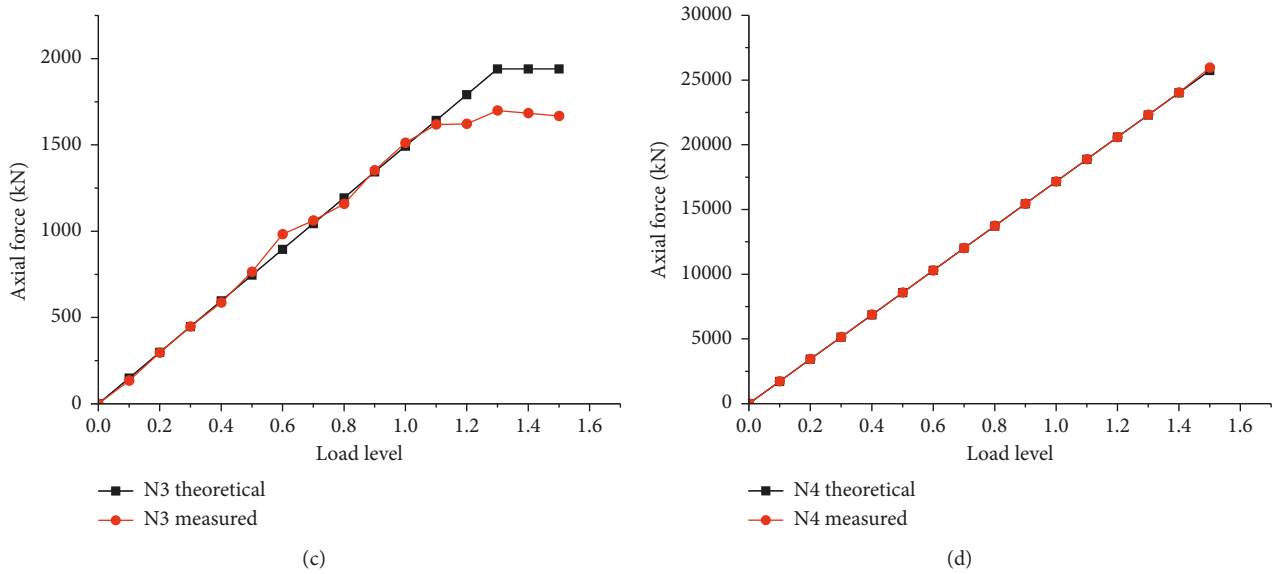

Figure 7: The theoretical and measured force of loading.

is the most important load. We think the unstable state is mainly caused by the bolted connections in the reaction frame. When it bears heavy load, a small slip may happen and finally lead to the unstable state during loading.

Due to the thickness of the joint, it is almost impossible for the joint to buckle. The axial forces are mainly tensile, and the moment makes the stress of the upper area much larger than the lower area. So the danger area is the upper area of the joint where all the members intersect. T4, T6, T20, T22, T26, T27, T36, and T37 are the test points in this area, and they are the most representative test points for the core area of the joint. The position of the important points in core area is marked in Figure 8(b), and the stress of the points during the loading procedure is shown in Figure 8(a).

The result shows that the von Mises stress is increasing linearly during the loading procedure. And all the branches and the core of the joint do not yield, they are still in the elastic area, and even the loading of N4 is increased to 1.5 times because the displacement and the deformation are relatively small and the von Mises stress of the core area is always less than the yield strength.

In the test, the stress of all the test points should never exceed the yield stress. The result is similar to the phenomenon of the test. The stress of some test points is not stable during the test. It is mainly caused by the instability of the load at level 1.0. Some test points near the stress concentration area are more easily affected by the instability of load. In Figure 8(a), we can find out that the decrease in the loading of N1 and N2 has different influence on different measuring point. T20, T22, and T37 have an obvious increase, while T27 decreases. The influence of the loading of N1 and N2 is discussed in Section 4.3.

4. Numerical Analysis

4.1. Model of the Test Specimen. The numerical analysis of the joint under complex loads is carried out by using the finite element method. The software used for the simulation is Abaqus. Abaqus has a good nonlinear mechanics analysis ability, and Wang et al. [20] carried out an analysis and optimized a cast-steel joint of a large reticulated shell structure by using Abaqus.

The 3D model of the joint is built and then imported with Abaqus. According to the experiment of the material property, the ideal elastic-plastic model is used to simulate the constitutive behavior of the material. The model is defined as a solid unit, and the material is G20Mn5QT, whose yield strength is 385 MPa, the tensile strength is about 555 MPa, and elastic modulus is 206000 N/mm^2. Poisson's ratio is 0.3. The plastic behavior of the material is defined by the kinematic hardening model.

Referred to the physical experiments, the boundary conditions of the numerical model are set as below: for N7 and N8, U1–U3, and UR1–UR3, totally 6 DOFs are fixed. N1–N6 are coupled to the control points, and the loads are loaded on the points. The load (N1–N5) and the reaction (N7 and N8) are listed in Table 5, and Figure 9 shows the model and meshing of the joint in Abaqus.

4.2. Comparison of the Simulation and Experiment. To validate the rationality of the FE model and the real physical model, the first step of the simulation is comparing the von Mises stress of the key points in the core area of the joint. In this step, the load of the FE model is similar that of the test, and the result of the key points can be seen in Figure 10.

Comparing the result of FE and the test, when the load level is lower than 1.0, the FE model matches the test result well. However, after 1.0 level, the test value of the stress is always smaller than the FE value. It is mainly because the loading of N1 and N2 is unstable around load level 1.0, and the real load of N3 is smaller than the theoretical value during load level 1.0–1.3. When the load increases stably,

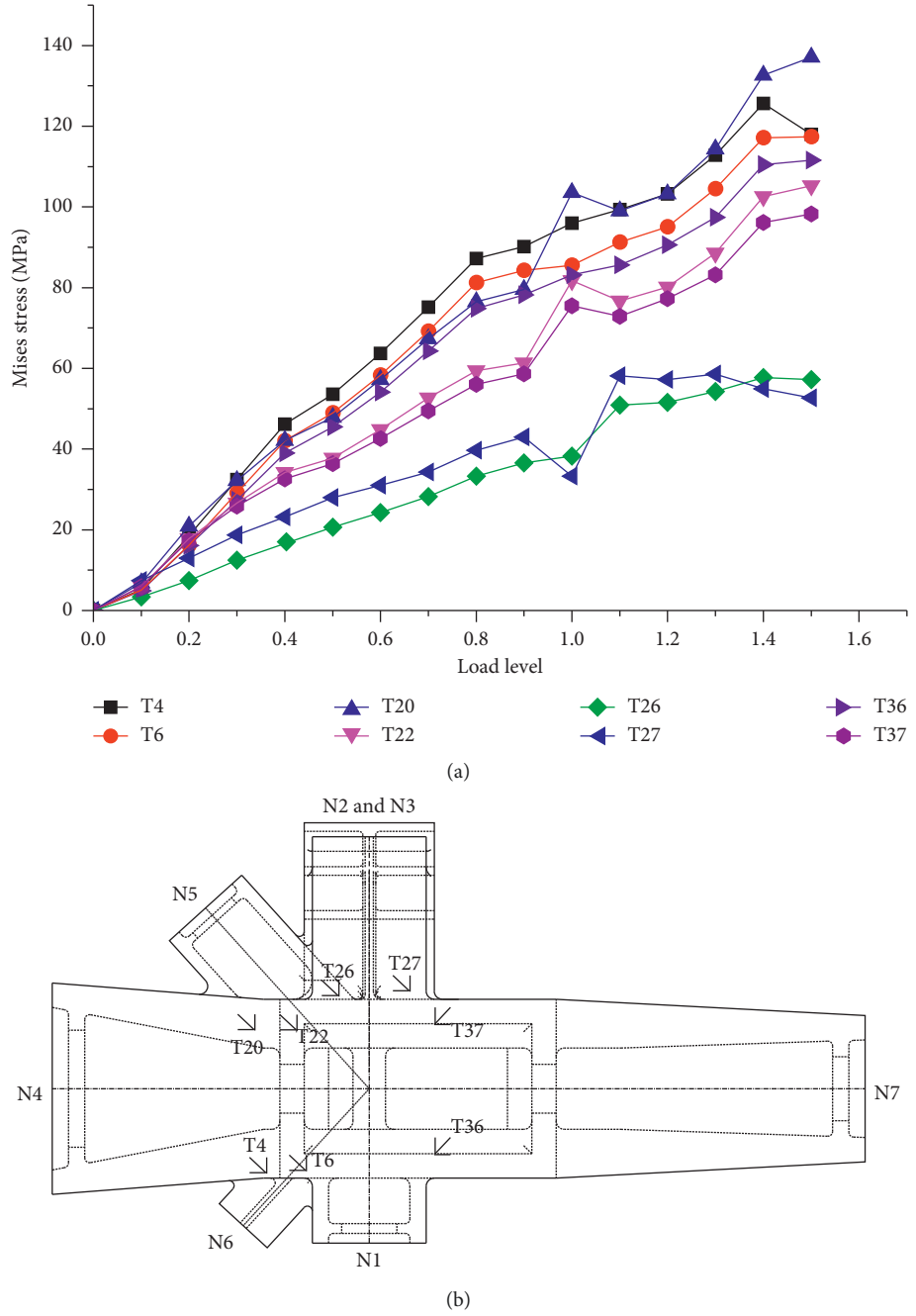

Figure 8: (a) Stress of the test points. (b) Position of the test points.

Table 5: The load and the reaction of the joint.

Unit number	Axial force of level 1.3 load (kN)	Axial force of level 1.0 load (kN)
N1	5068.7	3899.0
N2	3034.2	2334.0
N3	1939.6	1492.0
N4	22305.4	17158.0
N5	1313.0	1010.0
N7	15610.4	12008.0
N8	−7234.5	−5565.0

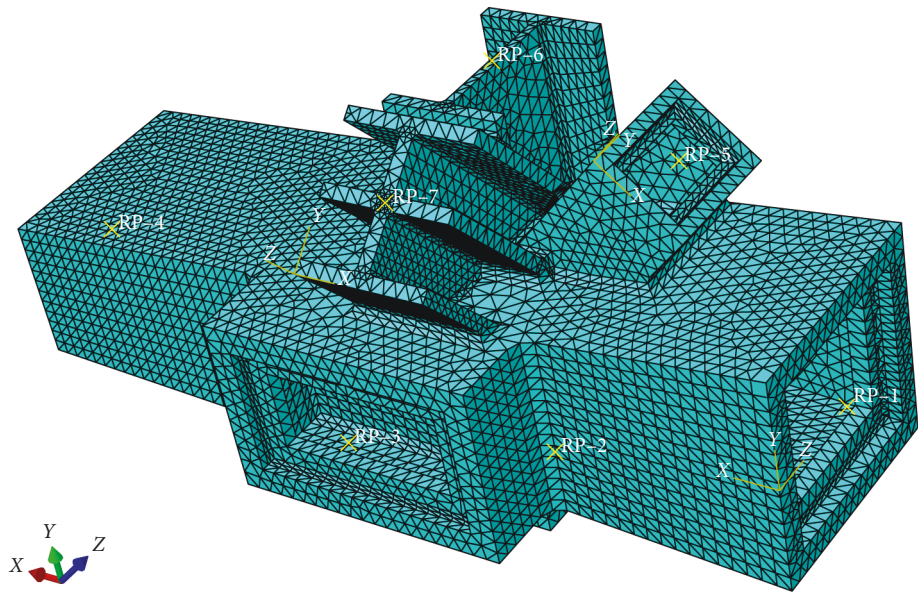

Figure 9: The model and meshing of the joint with Abaqus.

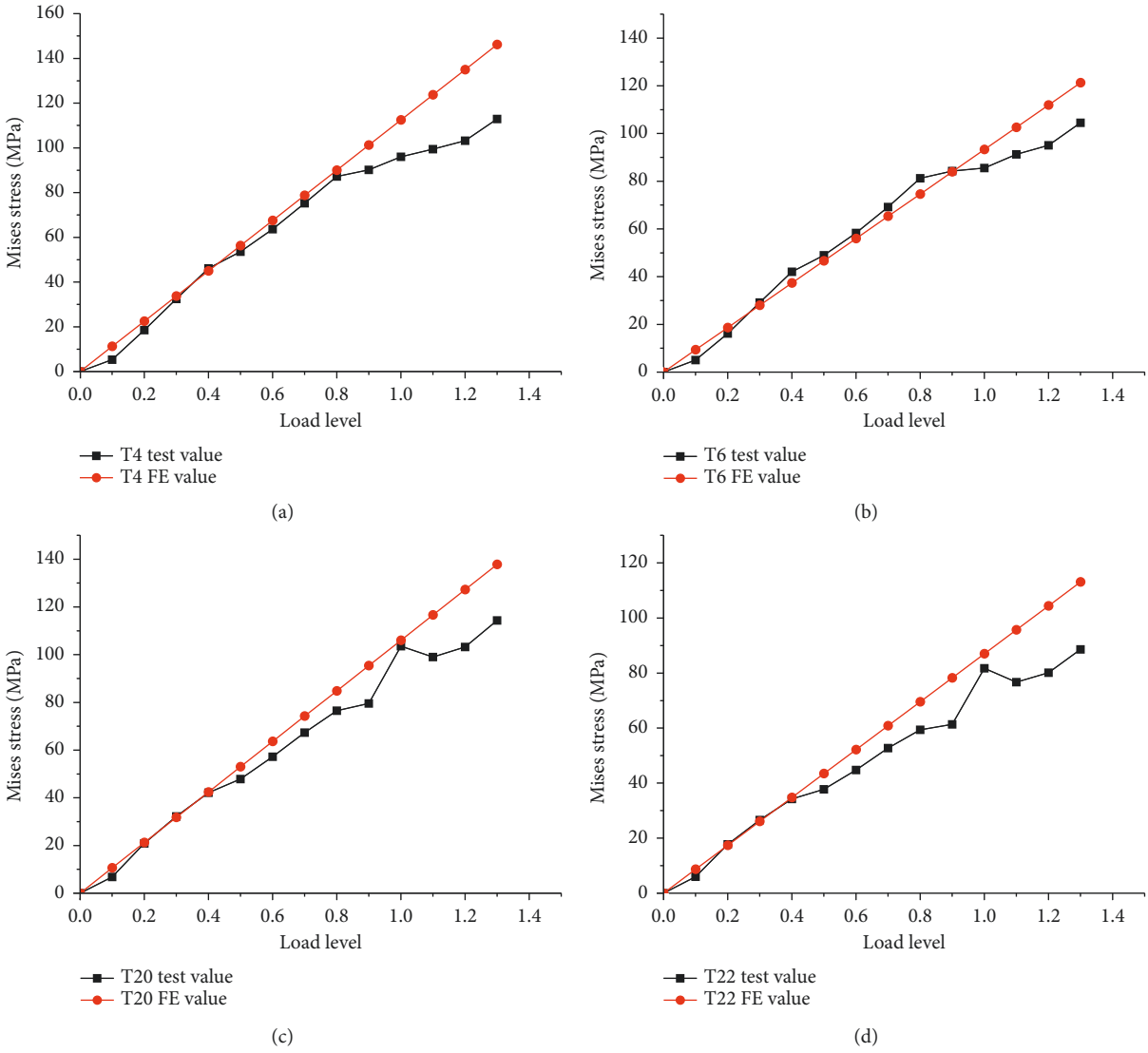

Figure 10: Continued.

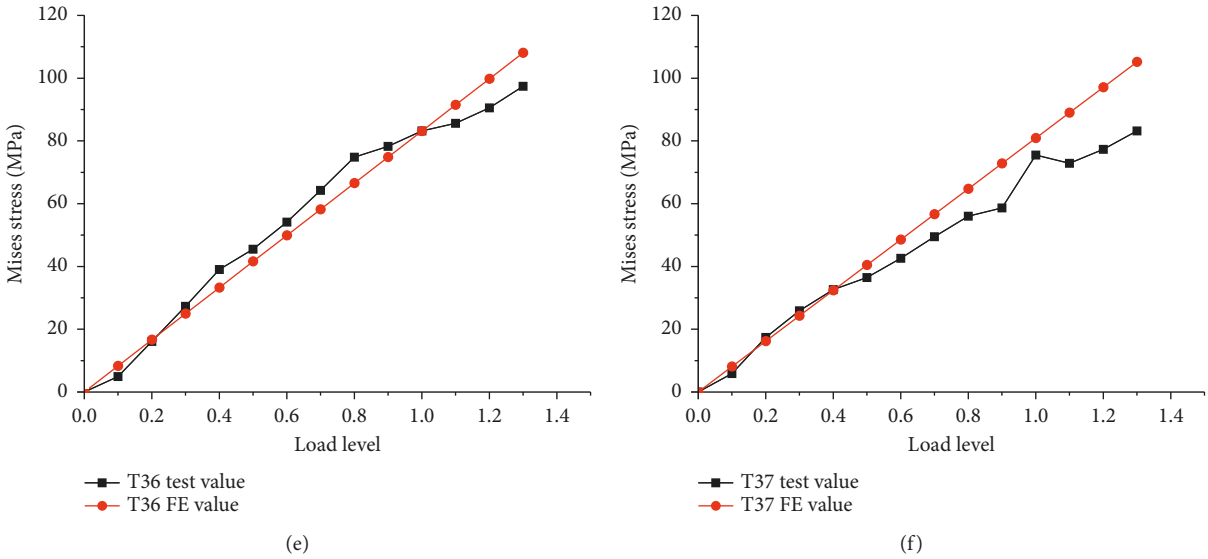

Figure 10: Comparing the test and FE simulation.

the result matches well. Considering the possible slip in the reaction frame at level 1.0, some equipment problem in the real test can also cause the difference between FE result and real test. It validates the effectiveness of the numerical analysis. For some connection areas of the member and joint (also the stress concentration area), the result behaves different. The FE value is larger than the test value. It is mainly caused by the sharp element in the meshing and finally leads to the concentration of stress in the FE model.

To validate the FE simulation, the boundary conditions should also be validated. Take the fixed branches N7 and N8 as examples, the reaction forces on the boundary is listed in Table 6.

The result validates the effectiveness of the numerical analysis. The error of the stress and reaction force between the real test and the FE simulation is acceptable. It allows the further use of the FE model. We can use the FE model to deal with the problem which is difficult to solve in the real test. Figure 11 is the stress nephogram of the joint under test load. Obviously, the joint is still in the elastic stage. Figures 12(a) and 12(b) are the z direction and magnitude displacement nephogram of the joint under the test load. In the real test, the displacement of the joint is very small. Considering the equipment problem, the measured result can only serve as a reference. The FE result of displacement shows that the maximum magnitude displacement is about 1.31 mm, close to the real test (1.35 mm).

4.3. Discussion of the Absence of the Secondary Load. In the test, due to the limitation of the equipment, some secondary loads are ignored. We can exert all the secondary load and discuss the influence of the absence of secondary load by using numerical analysis. Before we carry out the experiment, a preliminary FE analysis is used to confirm the secondary load. The main loads include the axial force of N1, N2, N3, N4, and the y direction moment of N4. The other moment and all the shear forces and torque are all considered as the secondary loads. In fact, the shear forces do have some influence on the result, but they are difficult to load. So they are also considered as secondary loads, and an enhancement coefficient is used to insure the safety of the joint. The load on N5 is also too small, and the cross section of N5 is also much smaller than the main branch. The result of preliminary FE analysis also proves that N5 can be ignored in the real test.

In the numerical analysis, we can exert all the loads we want without the limitation of the loading equipment. First, the absence of small moment only leads to about 5% of the change in stress, and similarly, the torque is meaningless for the distribution of the stress. But the absence of shear force will lead to a much bigger difference. As it is shown in Table 7, the difference can be up to more than 30%, so the shear of the joint should be taken into consideration through other methods to ensure the safety of the joint. The stress state under all secondary loads is similar to that under secondary shear. It also shows that shear is the most influential secondary load.

Although the secondary torque and moment do not make a difference for the stress distribution in core area of the joint, it will actually affect the stress concentration. The secondary torque only leads to about 1% difference for the stress in core area, but the maximum stress increases from 265.2 MPa to 364.2 MPa. It is even more than the influence of the shear. It shows that although the secondary load is very small, it can still have a great influence on the concentration of the stress. For the design of the joint, to avoid the stress concentration, all the secondary load should be taken into consideration. The influence for the stress concentration is shown in Table 8.

Table 6: The reaction forces for N7 and N8.

Unit number	Axial force, designed value (kN)	Axial force, FE result (kN)	Deviation (%)
N7	12008.0	11383.0	5.20
N8	−5565.0	−6410.6	15.19

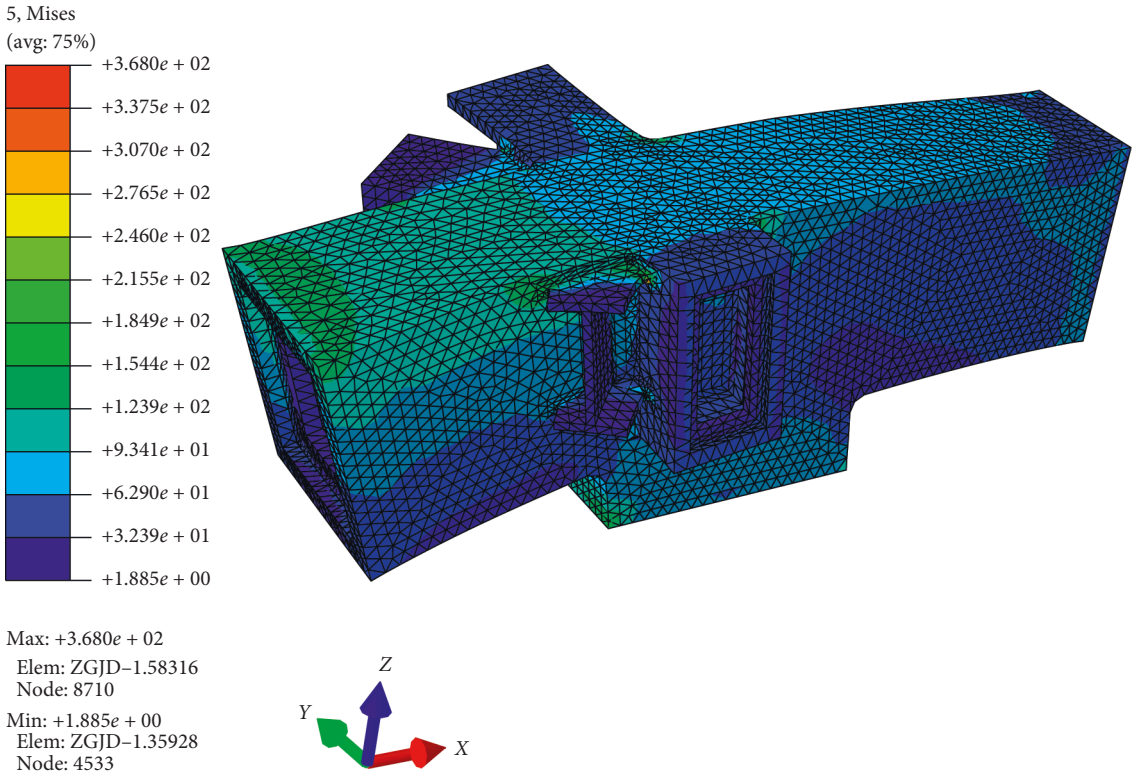

Figure 11: The stress nephogram under test load.

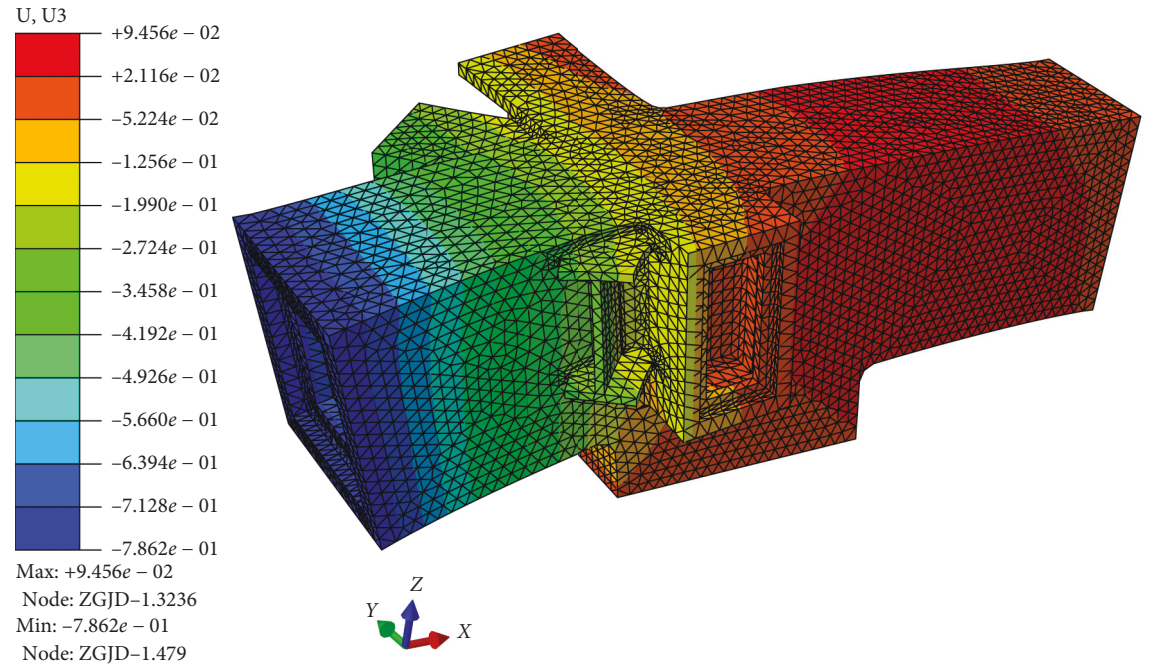

(a)

Figure 12: Continued.

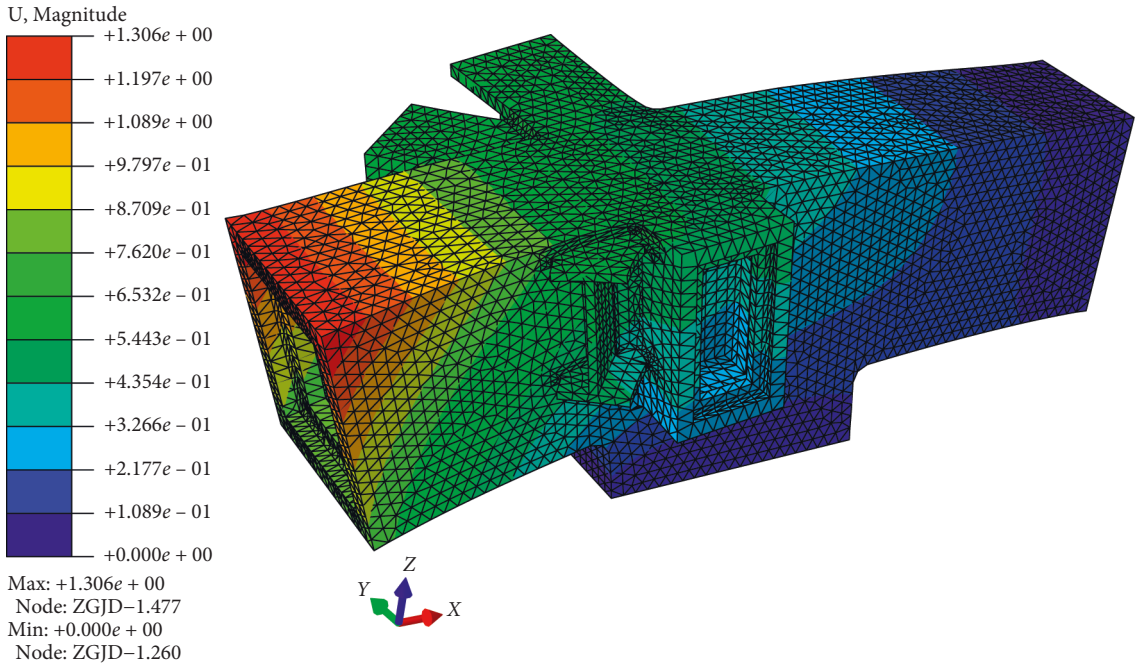

(b)

Figure 12: The displacement nephogram under test load. (a) Z direction displacement nephogram. (b) Magnitude displacement nephogram.

Table 7: The influence of the secondary load.

	T4	T6	T20	T22	T26	T27	T36	T37
Under test load (MPa)	112.46	93.26	106.01	86.95	54.83	81.87	83.15	80.91
With secondary moment (MPa)	118.46	98.64	100.44	82.54	55.17	83.72	89.64	78.77
Deviation (%)	5.33	5.77	−5.26	−5.06	0.62	2.25	7.80	−2.65
With secondary shear (MPa)	148.34	126.05	127.01	106.98	65.03	94.77	107.91	97.51
Deviation (%)	31.91	35.15	19.81	23.04	18.60	15.75	29.78	20.51
With secondary torque (MPa)	113.44	94.36	104.86	86.59	54.93	80.99	82.51	79.60
Deviation (%)	0.87	1.17	−1.08	−0.42	0.18	−1.08	−0.76	−1.62
With all secondary loads (MPa)	155.32	132.25	120.14	102.10	64.91	94.69	111.68	93.66
Deviation (%)	38.12	41.80	13.32	17.43	18.38	15.66	34.31	15.76

Table 8: The influence of secondary load in stress concentration.

	Under test load	With secondary moment	With secondary shear	With secondary torque	With all secondary loads
Maximum stress (MPa)	265.2	385.6	359.1	364.2	376.05
Location	—	Connection area of N6	Connection area of N6	Connection area of N6	Connection area of N6

It is obvious that the secondary shear forces will lead to the decrease in the capability of the joint. However, the secondary moment and torque still need more discussion. Although the secondary moment and torque sometimes have a positive influence on the stress of the joint (for example, the secondary moment for T20), but the secondary load will aggravate the stress concentration and finally lead to the plastic failure in the concentration area. The secondary moment and torque will also lead to the decrease in the capability.

The following is the discussion on the influence of secondary branches. It is obvious that the main branches of the joint are N4, N7, and N8. Both the size of the cross

Table 9: The influence of secondary load.

	T4	T6	T20	T22	T26	T27	T36	T37
Without secondary branches (MPa)	112.12	97.39	106.9	90.58	52.14	71.56	85.71	112.12
Under test load (MPa)	112.46	93.26	106.01	86.95	54.83	81.87	83.15	80.91
Deviation (MPa)	−0.34	4.13	0.89	3.63	−2.69	−10.31	2.56	−0.34

Table 10: Core area stress for different enhancement coefficients (MPa).

Test point	Under design load	With secondary shear	With all secondary loads	$a = 1.1$ $b = 1.1$	$a = 1.3$ $b = 1.3$	$a = 1.5$ $b = 1.3$	$a = 1.5$ $b = 1.5$	$a = 1.7$ $b = 1.5$
T4	112.457	148.34	155.32	123.79	146.31	168.74	168.84	191.3
T6	93.2618	126.05	132.25	102.04	120.61	139.6	139.19	158.19
T20	106.013	127.01	120.14	117.6	138.98	160.36	160.36	181.74
T22	86.9469	106.98	102.1	92.9	109.79	127.58	126.68	144.46
T26	54.8336	65.03	64.91	57.55	68.01	76.44	78.46	86.84
T27	81.8721	94.77	94.69	81.53	96.35	107.9	111.21	122.75
T36	83.1489	107.91	111.68	91.22	107.81	124.24	124.38	140.79
T37	80.9104	97.51	93.66	82.34	97.32	112.19	112.33	127.21

a is the enhancement coefficient of branch N4; b is the enhancement coefficient of N1–N3.

section and the value of the load of N4 are the biggest, and N7 is the continuation of N4. So N1, N2, N3, and N5 can all be considered as the secondary branches. The loads of all the secondary branches are axial compressive forces. To discuss the influence of the secondary branches, the result of the FE simulation without the secondary branches load is shown in Table 9.

T26 and T27 are on the branch N2 and a little bit away from the core area. So the absence of the loading of N3 leads to a great decrease in stress. But for the core area, for example, T6, T22, and T36, the absence of the secondary branches causes the increase in the converted stress. We can come to a conclusion that, for the core area of this joint, the axial force from the secondary branches is a positive factor for the capability of the core of the joint. The absence of the secondary branch will lead to the decrease in the capability of the joint. In fact, the real test also validates this opinion. In Figure 8(a), when the loading of N1 and N2 decreases (at load level 1.0), the stress in core area increases while T27 decreases.

4.4. Discussion of the Enhancement Coefficient for Real Test. Section 4.3 shows that the shear load will influence the converted stress of the joint greatly. To ensure the safety of the joint and the reliability of the test, in Section 2, we use an enhancement coefficient on the designed value of the load in the real test and enlarge the axial load and moment to replace the influence of the shear and other secondary load.

The enhancement coefficient is confirmed by FE simulation. Different enhancement coefficients are used in the model. The result of the FE simulation is listed in Table 10 and Figure 13 for the stress of core area under different enhancement coefficients. The stress under enhancement coefficients should always be larger than the stress under shear load and other secondary loads. Finally, we select 1.3 for N1–N3 and 1.5 for N4 as the values of enhancement coefficients based on the FE simulation and the advices of the designer. It is obvious that the enhancement coefficient can cover the absence of the shear and ensure the safety of the joint when it is difficult to load the secondary load.

4.5. Discussion of the Code Regulation. The code requests that the strength check should be as follows:

$$\sigma_{zs} = \sqrt{\frac{1}{2}\left[(\sigma_1 - \sigma_2)^2 + (\sigma_2 - \sigma_3)^2 + (\sigma_3 - \sigma_1)^2\right]},$$
$$\sigma_{zs} \le \frac{\beta_f f}{\gamma_{\mathrm{RE}}}, \tag{1}$$

where β_f is a coefficient for the converted stress, determined by the tension and compression situation in the area and γ_{RE} is the seismic adjustment coefficient. For this joint, $\beta_f = 1.0$ and $\gamma_{\mathrm{RE}} = 0.9$. If the joint can bear at least 2 times of the designed load in the real test or 3 times of the load in FE simulation, it is possible to ignore the stress check for the joint [13]. Under 3 times of the designed load, the FE model shows that member N4 starts to yield but the core area is still in the elastic stage. The stress concentration is much more obviously under 3 times of the load. We can also find that the stress of the core area can still pass the strength check provided by the code. The stress nephogram of the joint can be seen in Figure 14. The z direction and magnitude displacement of the joint can be seen in Figure 15. The magnitude displacement is about 5.92 mm, still very small relative to its size.

Under 4 times of the designed load, the core area of the joint still does not yield, and the upper area of member N4 yields. The core area does not completely yield even if the

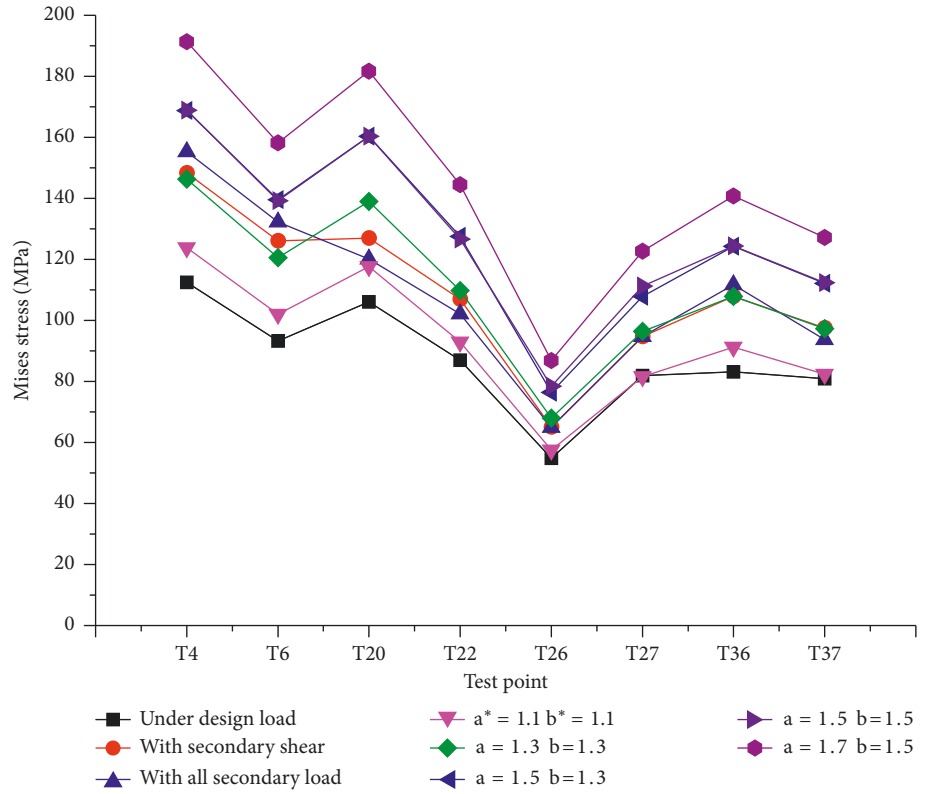

Figure 13: Core area stress for different enhancement coefficients.

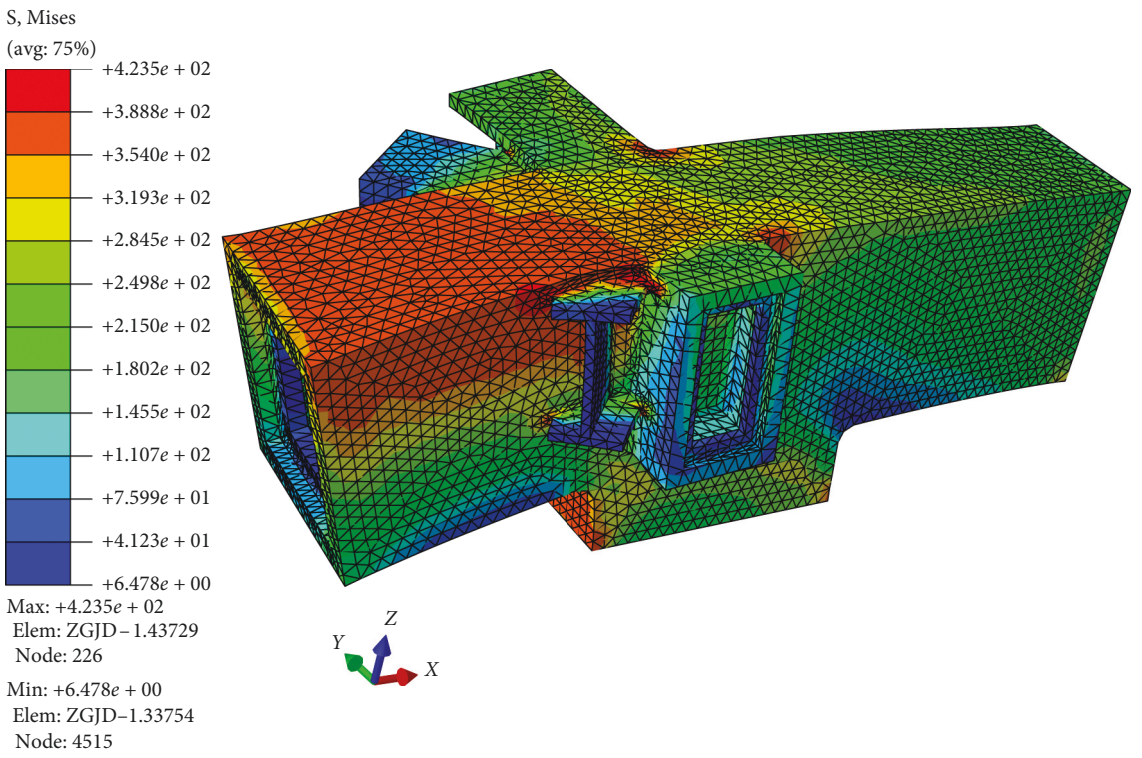

Figure 14: The stress nephogram under 3 times of the load.

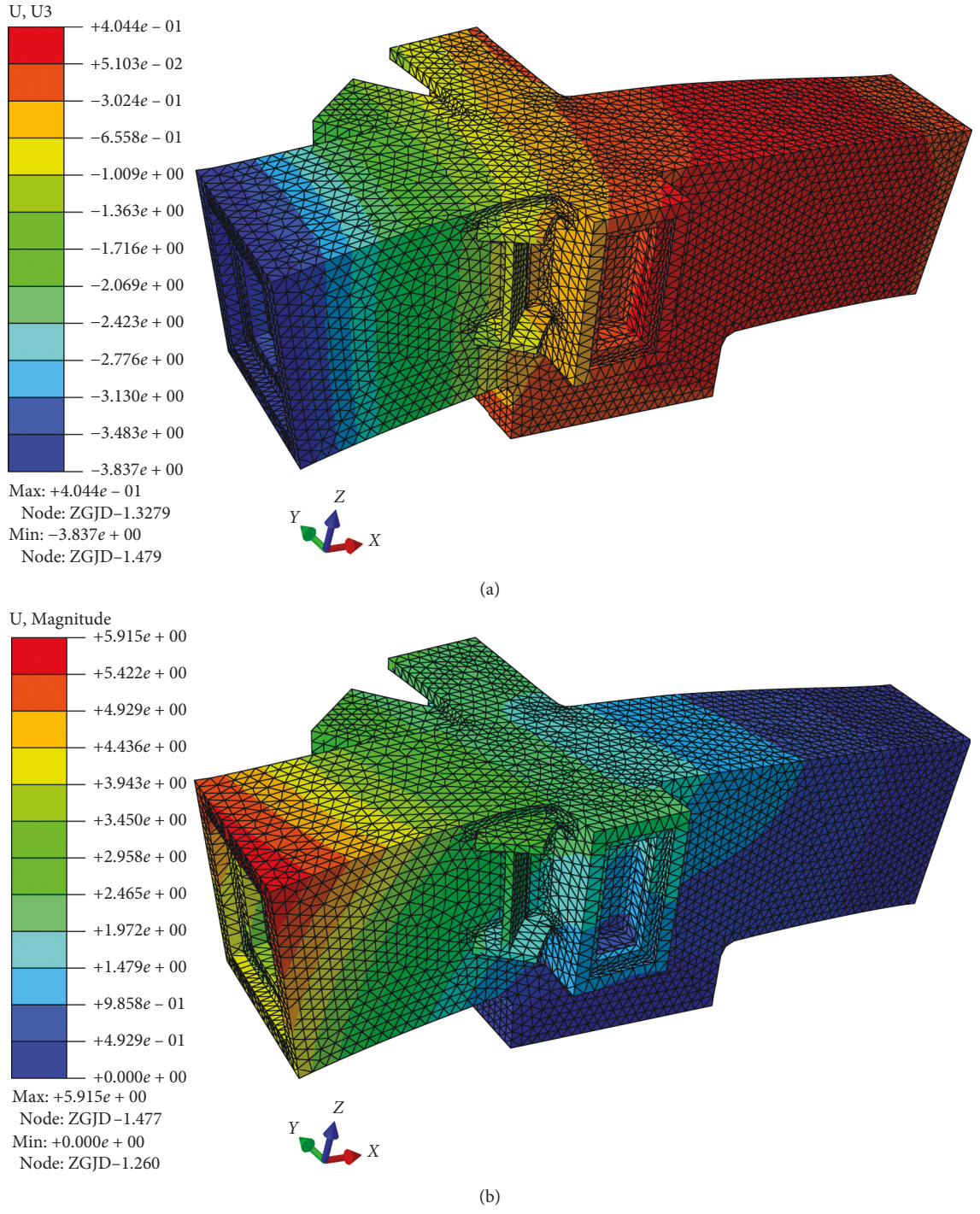

Figure 15: The displacement nephogram under 3 times of the load. (a) Z direction displacement nephogram. (b) Magnitude displacement nephogram.

branches has failed. It shows that the joint is safe enough for the current member. The capability of the joint is larger than the connected member. But the stress concentration is still a problem, the connection of the core area and branches N1 and N2 still needs a more rounded transition. The stress and displacement nephogram of the joint can be seen in Figures 16 and 17. The z direction displacement of N4 is still smaller than 10 mm in Figure 17(a).

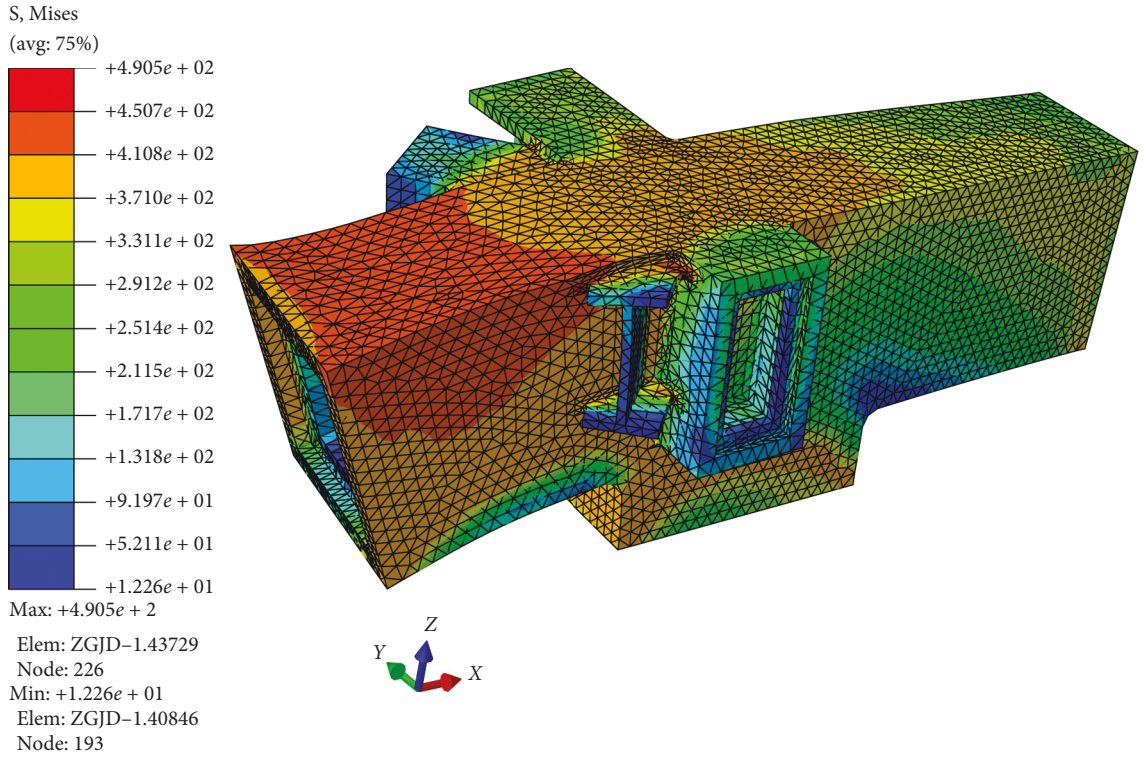

Figure 16: The stress nephogram under 4 times of the load.

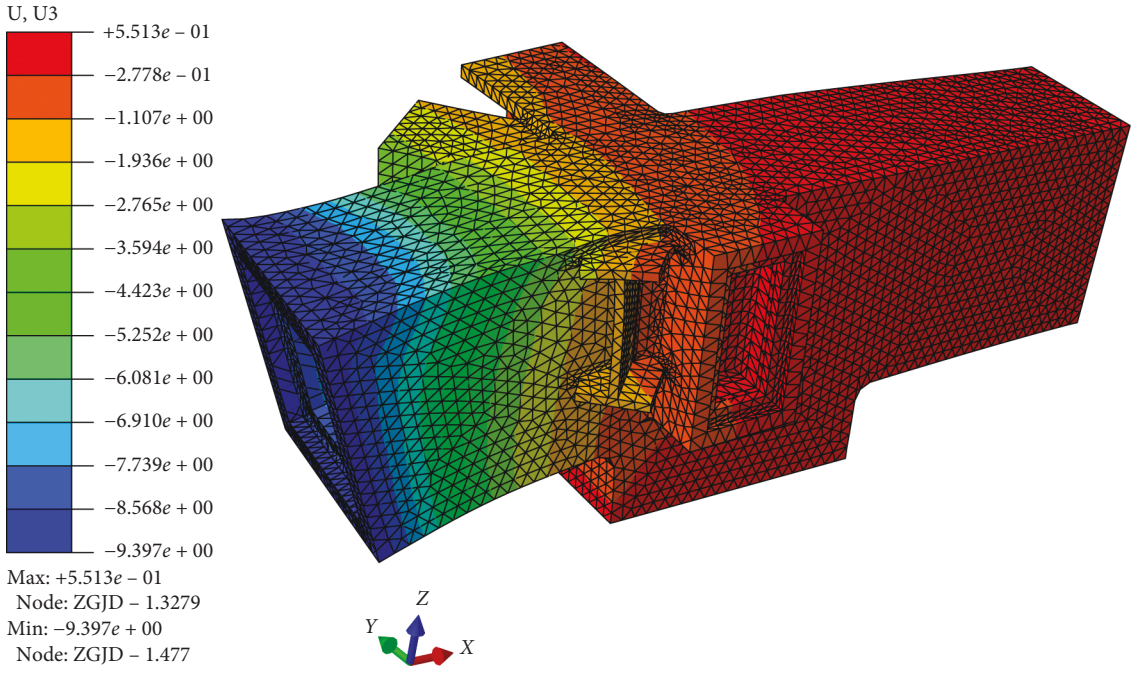

(a)

Figure 17: Continued.

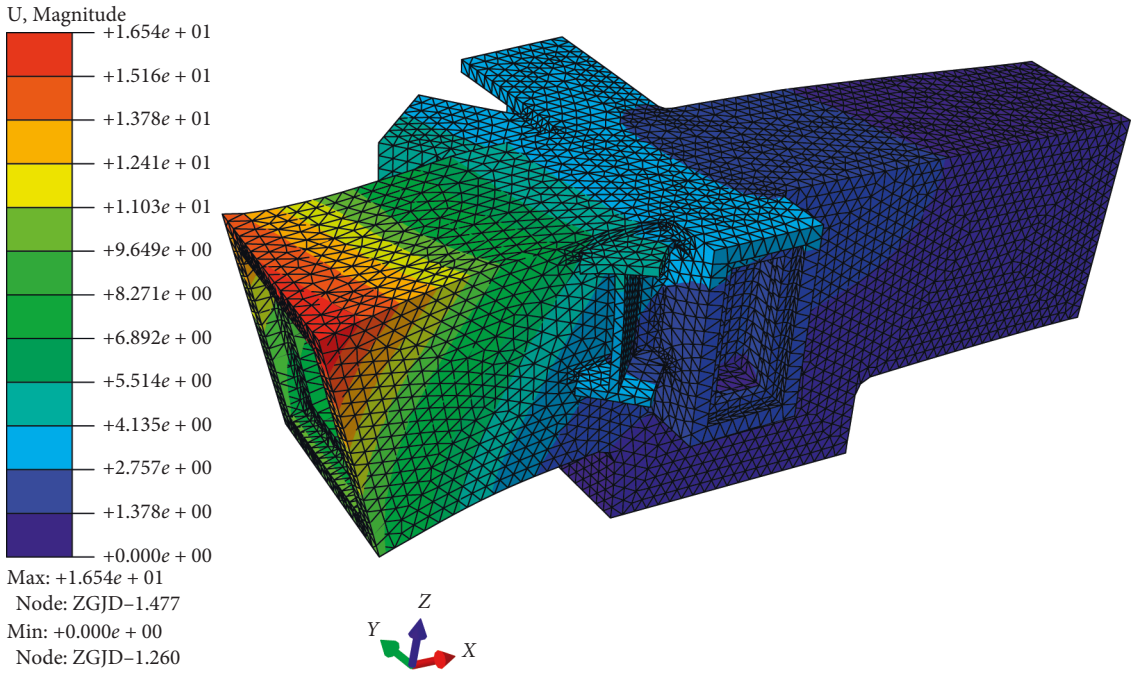

(b)

Figure 17: The displacement nephogram under 4 times of the load. (a) Z direction displacement nephogram. (b) Magnitude displacement nephogram.

5. Conclusions

The following conclusions can be made based on the test and the FE numerical analysis presented in this paper:

(1) In the test, the joint can bear the designed load and it lasts still in the elastic area, and under 3 times of the designed load, the joint does not undergo failure. The core area of the joint does not yield when the branch yields. The joint is safe enough for the project and compliance with the requirements of the code. The test also proves that the thick cast-steel joint (up to 150 mm) also behaves well under complex loads.

(2) The result of the FE and experiment shows that the FE simulation matches well. The stress distribution and the reaction forces are as expected. The method of testing the FE model through the experiment is acceptable, and we can obtain the result that is difficult to be obtained from the physical experiment due to the equipment and other limitations.

(3) The absence of secondary moment and torque does not really affect the stress distribution in core area much, but the secondary load can lead to a more serious stress concentration. The axial forces from the secondary branches increase the capability of the joint.

(4) The absence of shear leads to an obvious decrease in the stress. An enhancement coefficient can be used to enlarge the axial force and moment to cover the absence of the shear and ensure the safety and reliability of the model test.

(5) The joint has an obvious stress concentration at the connection area after 3 times of the designed load.

Data Availability

The data used to support the findings of this study are included within the article.

Conflicts of Interest

The authors declare that they have no conflicts of interest.

Authors' Contributions

Bin Yang and Ke Lei conceptualized and designed the study. Dayu Zhu and Binghan Zhang participated in the data acquisition. Binghan Zhang performed data analysis and interpretation and drafted the manuscript. Tiankai Wu revised the manuscript critically for important content. Binghan Zhang, Bin Yang, Tiankai Wu, Dayu Zhu, and Ke Lei approved the version of the manuscript for publication.

References

[1] W. Bao, L. T. Xing, and J. H. Qiu, "The use of cast steel in steel structure," *Advanced Materials Research*, vol. 183–185, pp. 1918–1922, 2011.

[2] H. Han, M. J. Liu, Y. Lu, and S. S. Zhao, "Experimental and simulation study on seismic behavior of beam-column joints with cast steel stiffener," *Journal of Structural Engineering*, vol. 142, no. 7, article 04016030, 2016.

[3] L. Tong, Y. Chen, Y. Chen, and C. Fang, "Cyclic behaviour of beam-to-column joints with cast steel connectors," *Journal of Constructional Steel Research*, vol. 116, pp. 114–130, 2016.
[4] X. Zhao, Z. Shen, and Y. Chen, "Some key techniques for the design of connections of structural steel casting," *Structural Engineer*, vol. 25, no. 4, 2009, in Chinese.
[5] Q. Han, Q. Guo, Y. Yin, and Y. Xing, "Fatigue behaviour of G20Mn5QT cast steel and butt welds with Q345B steel," *International Journal of Steel Structures*, vol. 16, no. 1, pp. 139–149, 2016.
[6] W. Du, Y. Sun, and M. Yang, "Bearing capacity of the cast-steel joint with branches under eccentric load," *Journal of Constructional Steel Research*, vol. 135, pp. 285–291, 2017.
[7] P. Broughton, R. Hayes, A. Wood, and S. Komaromy, "Cast steel nodes for the EKOFISK 2/4J jacket," *Proceedings of the Institution of Civil Engineers—Structures and Buildings*, vol. 122, no. 3, pp. 266–280, 1997.
[8] H. Chen, Q. Zhang, and H. Jin, "Experimental study on fatigue properties of cast-steel joints of Hangzhou Bay sightseeing tower," *Journal of Building Structures*, vol. 30, no. 5, pp. 149–154, 2009, in Chinese.
[9] J. Lu, H. Liu, Z. Chen, and L. Bisby, "Experimental investigation of the residual mechanical properties of cast steels after exposure to elevated temperature," *Construction and Building Materials*, vol. 143, pp. 259–271, 2017.
[10] L. Tong, Y. Zhang, L. Zhang, H. Liu, Z. Zhang, and R. Li, "Ductility and energy dissipation behavior of G20Mn5QT cast steel shear link beams under cyclic loading," *Journal of Constructional Steel Research*, vol. 149, pp. 64–77, 2018.
[11] W. Du, Z. Sun, B. Gao, and S. Dong, "Finite elment analysis of a cast-steel joint with three branches in tree-like structure," *Journal of Building Structures*, vol. 35, pp. 89–93, 2014, in Chinese.
[12] J. Song, L. Yang, Q. Zhang, and Y. Wang, "Full-scale experimental study on cast steel joint of Hangzhou international conference center," *Journal of Building Structures*, no. S1, pp. 98–110, 2007, in Chinese.
[13] CECS 235:2008, *Technical Specification for Application of Connections of Structural Steel Casting*, China Association for Engineering Construction Standardization, Beijing, China, 2008, in Chinese.
[14] M. Ramu, V. P. Raja, and P. R. Thyla, "Establishment of structural similitude for elastic models and validation of scaling laws," *KSCE Journal of Civil Engineering*, vol. 17, no. 1, pp. 139–144, 2013.
[15] B. C. Chang, G. M. Kim, I. J. Kwahk, and Y. S. Chung, "Seismic performance investigation of RC piers with lap-spliced longitudinal bars as to aspect ratio," *KSCE Journal of Civil Engineering*, vol. 18, no. 6, pp. 1768–1779, 2014.
[16] Z. Wang, X. Zhao, Y. Chen, and Z. Shen, "Bearing capacity of the special-shape cast steel joint for Shanghai South railway station," *China Civil Engineering Journal*, vol. 41, no. 1, 2008, in Chinese.
[17] Y. Su, X. Li, and X. Wu, "Evaluation of load-bearing performance of existing cast steel node," *Civil Engineering Journal*, vol. 3, no. 2, 2017.
[18] K. Liu, B. Liu, Z. Wang, G. Wang, and C. G. Soares, "An experimental and numerical study on the behaviour of tubular components and T-joints subjected to transverse impact loading," *International Journal of Impact Engineering*, vol. 120, pp. 16–30, 2018.
[19] A. Jahangiri, F. Behnamfar, and M. Jahangiri, "Introducing the innovative post-tensioned connection with the rigid steel node," *KSCE Journal of Civil Engineering*, vol. 21, no. 4, pp. 1247–1255, 2016.
[20] F. Wang, Z. F. Luo, and S. H. Mo, "The application of ABAQUS in cast-steel joints elastic-plastic analysis," *Applied Mechanics and Materials*, vol. 351-352, pp. 854–859, 2013.